Shear wave splitting and V_P/V_S variations before and after the Efpalio earthquake sequence, western Gulf of Corinth, Greece

D. Giannopoulos,[1] E. Sokos,[1] K. I. Konstantinou[2] and G-Akis Tselentis[1,3]

[1]*Seismological Laboratory, University of Patras, Rio 26504, Greece*
[2]*Department of Earth Sciences, National Central University, Jhongli 320, Taiwan. E-mail: kkonst@cc.ncu.edu.tw*
[3]*Institute of Geodynamics, National Observatory of Athens, Athens 11810, Greece*

SUMMARY

On 2010 January 18 and 22, two earthquakes of M_W 5.3 and 5.2, respectively, occurred near the town of Efpalio on the western Gulf of Corinth. We performed a shear wave splitting analysis using the cross-correlation method and calculated V_P/V_S ratios for events that occurred in the epicentral area of the Efpalio earthquakes, between 2009 January and 2010 December. The data analysis revealed the presence of shear wave splitting in the study area, as well as variations of the splitting parameters and V_P/V_S ratios. The average values of time-delay, fast polarization direction and V_P/V_S ratio for the time period before the Efpalio earthquakes, were calculated at $2.9 \pm 0.4 \, \mathrm{ms \, km^{-1}}$, $92° \pm 10°$ and 1.76 ± 0.04, respectively, while after the occurrence of the earthquakes, including the aftershock sequence, they were calculated at $5.5 \pm 0.5 \, \mathrm{ms \, km^{-1}}$, $82° \pm 9°$ and 1.88 ± 0.04. A few months after the occurrence of the Efpalio earthquakes, the mentioned splitting parameters were calculated at $3.6 \pm 0.4 \, \mathrm{ms \, km^{-1}}$ and $83° \pm 9°$. V_P/V_S ratio exhibited a mean value of 1.87 ± 0.04. The mean fast polarization directions were in general consistent with the regional stress field, almost perpendicular to the direction of the extension of the Gulf of Corinth. The observed increase in the time-delays and V_P/V_S ratios after the Efpalio earthquakes indicates changes in the crustal properties, which possibly resulted from variations in the pre-existing microcrack system characteristics. We suggest that a migration of fluids in the form of overpressured liquids, which are likely originated from dehydration reactions within the crust, was triggered by the Efpalio earthquakes and caused the observed variations. The findings of this work are consistent with those of previous studies that have indicated the presence of fluids of crustal origin in the study area.

Key words: Seismic anisotropy; Wave propagation; Crustal structure.

1 INTRODUCTION

Shear wave splitting is a phenomenon in which shear waves are separated into two components with different polarization directions and propagation velocities. This can occur during shear wave propagation through an anisotropic medium (Crampin & Chastin 2003; Crampin & Peacock 2005). The two splitting parameters that can be measured through shear wave data processing are the polarization direction φ of the fast component of the shear waves, and the time-delay dt between the two components. Changes in the splitting parameters have been observed worldwide in relation to earthquakes reflecting changes in the anisotropic characteristics of the medium and/or the stress field (Gao & Crampin 2004; Crampin & Gao 2012). These variations in the shear wave splitting parameters, and specifically variations in shear wave splitting time-delays before and after strong earthquakes, are quite complicated and have often been the subject of debate. Such cases are Peacock *et al.* (1988), Aster *et al.* (1990), Crampin *et al.* (1990, 1991), Seher & Main (2004), Peng &

Ben-Zion (2005), Munson *et al.* (1995), Liu *et al.* (2004, 2005) and Crampin & Gao (2005). According to Crampin (1999), the principal driving mechanism for these changes is fluid migration along pressure gradients between closely spaced microcracks and pores at different orientations to the stress field. The parameters that control changes to microcrack geometry also control the splitting of shear waves, so that changes in deformation can be directly monitored by analysing the shear wave splitting, making shear wave splitting phenomenon an important tool for determining crustal deformation processes.

The Gulf of Corinth is a continental rift which separates the central Greek mainland from Peloponnese. The rift is approximately 120 km long and 10–20 km wide, with a WNW–ESE orientation, extending from the Gulf of Patras in the west, to the Gulf of Alkionides in the east. The Gulf of Corinth is considered as one of the most active extensional intracontinental rifts in the world (Armijo *et al.* 1996), with the geodetically measured rates of extension varying from ~5 mm yr^{-1} at the eastern part, to ~15 mm yr^{-1} at the

western part (Briole *et al.* 2000; Avallone *et al.* 2004). Several studies aimed at interpreting the cause of the high extension rates of the Corinth Gulf. Some have linked the rift formation to the westward motion of the Anatolian microplate and the propagation of the North Anatolian fault (Jackson 1994; Le Pichon *et al.* 1995). Other studies related the rift formation to the roll-back of the subducting African Plate (Le Pichon & Angelier 1979; Hatzfeld *et al.* 1997) and others to a combination of both processes (McClusky *et al.* 2000; Doutsos & Kokkalas 2001). Anisotropy studies of the deep lithosphere, comprising the lower crust and lithospheric mantle have also been performed, improving the knowledge and understanding of the dynamics of extension in parts of the backarc Aegean area, like the Gulf of Corinth (e.g. Hatzfeld *et al.* 2001; Edrun *et al.* 2011; Evangelidis *et al.* 2011 among others). Neotectonic faults (e.g. Jackson *et al.* 1982; Doutsos & Poulimenos 1992), earthquake focal mechanism solutions (e.g. Rigo *et al.* 1996; Bernard *et al.* 1997) and GPS measurements (e.g. Clarke *et al.* 1998) indicate an approximately N–S direction of extension. The high extension rates in the Gulf of Corinth are accompanied by a high level of microseismic activity, especially at the western part, which is characterized by frequent earthquake swarms and also by the occurrence of large earthquakes across the whole section of the gulf (Bourouis & Cornet 2009). Although the Gulf of Corinth is geographically limited, numerous on- and offshore earthquakes with magnitudes up to 7 were instrumentally recorded or historically reported (Papadopoulos 2000). Some of the large and destructive earthquakes that occurred during the last three decades are the Alkionides seismic sequence in 1981 involving three strong events of M_S 6.7, 6.4 and 6.4 (Jackson *et al.* 1982), the M_S 5.9 Galaxidi earthquake in 1992 (Hatzfeld *et al.* 1996), the M_S 5.4 Patras earthquake in 1993 (Karakostas *et al.* 1994; Tselentis *et al.* 1994) and the M_S 6.2 Aigion earthquake in 1995 (Tselentis *et al.* 1996; Bernard *et al.* 1997).

On 2010 January 18 (GMT 15:56) an earthquake of M_W 5.3 (Efp1) occurred near the town of Efpalio along the northern coast of the western Gulf of Corinth. Four days later, on January 22, about 5 km to the northeast from the first earthquake another M_W 5.2 event occurred (GMT 00:46; Efp2). The two main shocks and the spatiotemporal evolution of the Efpalio sequence were thoroughly studied by Ganas *et al.* (2013), Sokos *et al.* (2012) and Karakostas *et al.* (2012) among others. According to Sokos *et al.* (2012), the January 18 and 22 earthquakes were located at hypocentral depths of 6.6 and 8.0 km, respectively. Both events exhibit normal faulting along E–W trending planes. More specifically, the first event was related with a south-dipping fault plane (strike 102°, dip 55°), while the second event seemed to be related with a north-dipping plane (strike 282°, dip 52°; Sokos *et al.* 2012). These structures may coincide with already mapped surface traces of faults. The surface trace for the south-dipping fault of the first event is very well correlated with the Trikorfo-Filothei south-dipping fault while the extrapolated surface termination of the assumed causative fault for the second event is located offshore, close to the north-dipping fault mapped by Papanikolaou *et al.* (1997).

The purpose of this paper is to study the temporal variability of the shear wave splitting parameters and V_P/V_S ratios during the years 2009–2010 in the epicentral area of the Efpalio earthquakes as well as to investigate the factors that caused these variations. After describing the available data and the methods of the shear wave splitting analysis and the calculation of V_P/V_S ratios which we followed, we will present and discuss the measured parameters. We provide evidence that the observed changes of the aforementioned parameters were possibly caused by temporally evolving conditions in the upper crust. These variations are investigated by comparing

measurements from event doublets that have occurred at different time periods (before and after the Efpalio earthquakes) but at the same focal area. Finally, we attempt to interpret the causative factors of the observed temporal variations, associated with the Efpalio earthquakes occurrence, in terms of the regional stress field and the possible involvement of fluids.

2 DATA AND METHODOLOGY

For the purpose of this study, we used recordings from six permanent broad-band stations, located on the western part of the Gulf of Corinth, operated under the framework of the Hellenic Unified Seismological Network (HUSN) and the Corinth Rift Laboratory (CRL, http://crlab.eu/). Efpalio (EFP) and Sergoula (SERG) stations were deployed by the University of Patras Seismological Laboratory (UPSL, http://seismo.geology.upatras.gr/) in cooperation with Charles University in Prague (http://geo.mff.cuni.cz/) while the other four seismic stations of Trizonia (TRIZ), Kalithea (KALE), Rodini (ROD) and Lakka (LAKA) were deployed by the CRL in cooperation with the Seismological Laboratory of Athens University (NKUA, http://dggsl.geol.uoa.gr/).

The waveform data studied here consists of the background seismicity and aftershocks of the M_W 5.3 and 5.2 Efpalio earthquakes, recorded from 2009 January until 2010 December. The location parameters of the studied events were provided by the Institute of Geodynamics — National Observatory of Athens (IG-NOA, http://bbnet.gein.noa.gr/). The mean location errors in the horizontal and vertical directions did not exceed ±0.6 and ±1.9 km, respectively. In Fig. 1(a) general map of western Gulf of Corinth is presented, showing the seismic stations (triangles) and the events (coloured circles) from which valid splitting results were obtained.

The estimation of the splitting parameters was performed using a cross-correlation method (Ando *et al.* 1983). Before applying the method, we manually picked *P*- and *S*-wave arrivals. The seismograms were interpolated to 200 samples s^{-1}, integrated to displacement and then bandpass filtered between 1 and 10 Hz. The measurement window for each waveform was defined in the following way: the start of the window was fixed 0.05 s before the *S*-wave arrival while the endpoint was adjusted each time until the value of cross-correlation coefficient C between the fast and slow components was maximized. According to the cross-correlation method, both horizontal seismograms are rotated in the horizontal plane at 1° increment of azimuth (α) from −90° to 90°. Then, for each azimuth, the cross-correlation coefficient C is calculated between the two orthogonal seismograms, for a range of time-delays (τ) in a selected time window. When the absolute value of C reaches a maximum, the corresponding values of azimuth (α) and time (τ) are chosen as the fast polarization direction and the time-delay between the separated shear waves, respectively. The measurement's uncertainty is estimated using a *t*-test at a 95 per cent confidence level on the values of C as described by Kuo *et al.* (1994). We accept as valid the splitting measurements which conform to the following criteria: (i) the C value is larger than 0.80, (ii) the signal-to-noise ratio is larger than 2.5, (iii) the change of the measured d*t* is less than 0.02 s when the window size is varied by ±0.02 s and (iv) the change of the measured φ is less than 10° when the window size is varied by ±0.02 s. An example of a valid splitting measurement is shown in Fig. 2. The recordings, from which we calculated the splitting parameters, are derived from seismic events all located within the effective shear wave window (Crampin & Gao 2006) of every station (incidence angle ≤45°) at depths ranging from 4 to
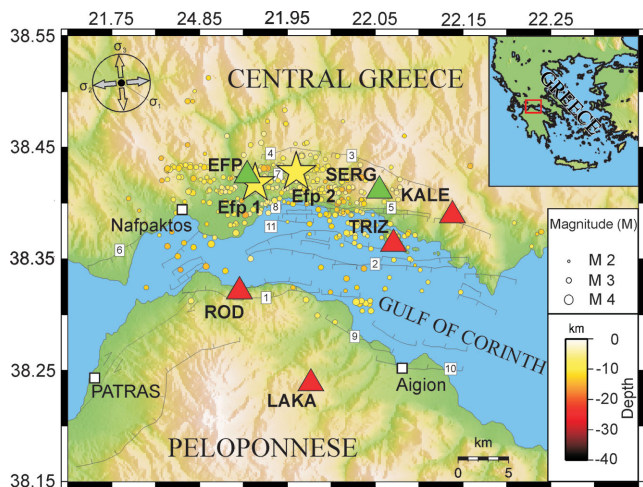
Figure 1. Map of the study area in western Gulf of Corinth. Seismic stations used for the shear wave splitting analysis are shown as triangles, where green and red colours signify stations operated by the University of Patras Seismological Laboratory (UPSL) and Corinth Rift Laboratory (CRL) in collaboration with the Seismological Laboratory of Athens University (NKUA), respectively. The seismic events (coloured circles) from which the valid splitting results were obtained, the Efpalio earthquakes epicentres (Efp1 and Efp2 as stars), major cities (squares) and major fault traces of the area are also shown. As in Doutsos & Poulimenos (1992), Flotté *et al.* (2005), Papanikolaou *et al.* (1997) and Valkaniotis (2009) the major faults shown are: 1 = Psathopyrgos, 2 = Trizonia, 3 = Trikorfo, 4 = Filothei, 5 = Marathia, 6 = Antirio, 7 = Drosato, 8 = Efpalio, 9 = Selianitika, 10 = Aigion and 11 = off shore fault related to Efpalio sequence and other on- and off-shore faults. The orientation of the principal stress axes after Kokkalas *et al.* (2006) is shown at the top left-hand corner. The depths of the events are colour coded according to the colour scale (bottom-right). The diameters of the circles are proportional to the magnitudes.

15 km. The local magnitudes of the events used in our analysis varied between 2.1 and 3.3.

Following the approach of Nur (1972), under the assumption of linear ray paths, we calculated an average V_P/V_S ratio using the estimated travel times at each station for all the events that satisfied the splitting criteria:

$$\frac{V_P}{V_S} = \frac{t_S}{t_P} \qquad (1)$$

with $t_S = T_S - T_O$ and $t_P = T_P - T_O$, where T_S and T_P are the arrival times of the S and P waves, respectively. The calculated V_P/V_S ratios are then compared to the corresponding time-delays, giving additional information about the average properties of the medium along the ray paths.

3 RESULTS

In order to present the findings in a more efficient way, we separated the 2-yr-long data set into three subperiods. The time period before the occurrence of the Efpalio earthquakes, from 2009 January until 2010 January 18 (hereafter called 'Period I'), the period that began soon after the occurrence of the earthquakes, including the aftershock sequence, from 2010 January 22 until the end of 2010 June (hereafter called 'Period II'), and the remaining time period until the end of 2010 (hereafter called 'Period III'). Another important factor for an efficient presentation and interpretation of the measurements, in addition to the previous temporal separation of the data, is the spatial distribution of the studied seismic events. For
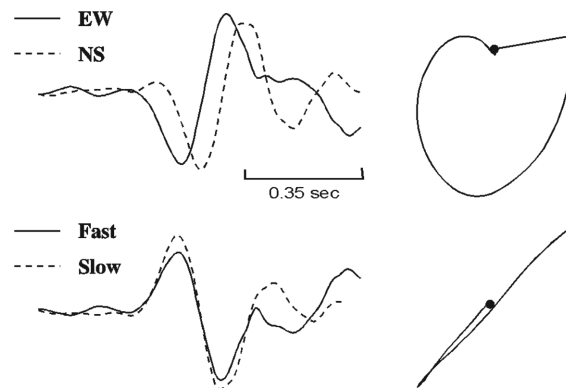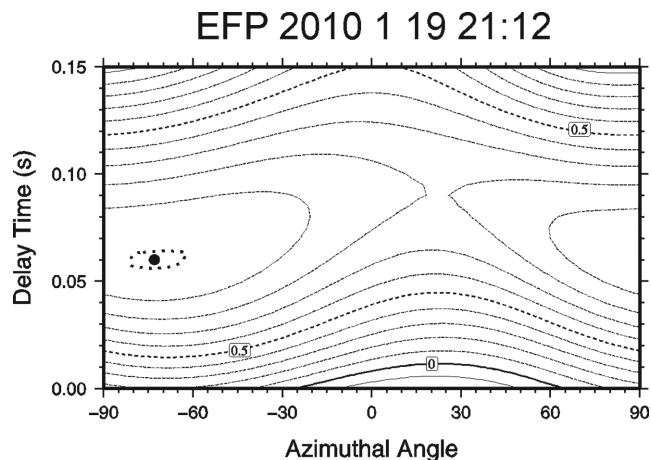

Figure 2. An example of a valid splitting measurement of the shear waves recorded at the EFP station for an event that occurred in 2010 January 19. Upper panel: Contour diagram of the cross-correlation coefficient in the $(\varphi, \mathrm{d}t)$ space. The preferred solution of $(\varphi, \mathrm{d}t)$ corresponding to the maximum value (dot) is shown within the 95 per cent confidence region (dotted line). Lower panel: Superposition of the horizontal components (upper traces), and the corrected fast and slow components (lower traces) once the splitting effects have been removed. Particle motions are shown to the right of each subpanel.

this reason, we also grouped the data spatially to that located inside and very close to the rupture areas of the Efpalio earthquakes and those located outside. We calculated the approximate dimensions of the rupture areas based on the empirical relationship between the moment magnitude and the rupture area proposed by Wells & Coppersmith (1994). Since the aftershock activity of the Efpalio earthquakes seemed to expand slightly into the surrounding area beyond the calculated boundaries of the rupture areas (see Sokos *et al.* 2012, Fig. 1b), for selecting the data which were close to the rupture area, we broadened the selection boundaries in accordance with the distribution of the early aftershocks during the first ∼30 d after the Efpalio earthquakes as it is shown by Sokos *et al.* (2012) (see Fig. 3). By separating the studied time period and the data in these ways, considering the occurrence of the Efpalio earthquakes as a significant time point of our study, we are actually focusing on time periods in which the properties of the upper crust possibly exhibit different characteristics.

After the shear wave analysis, using the whole data set, we obtained 439 valid splitting measurements derived from 416 seismic events. Specifically, we obtained 108 valid measurements for the Period I, 257 for the Period II and 74 for the Period III. A first
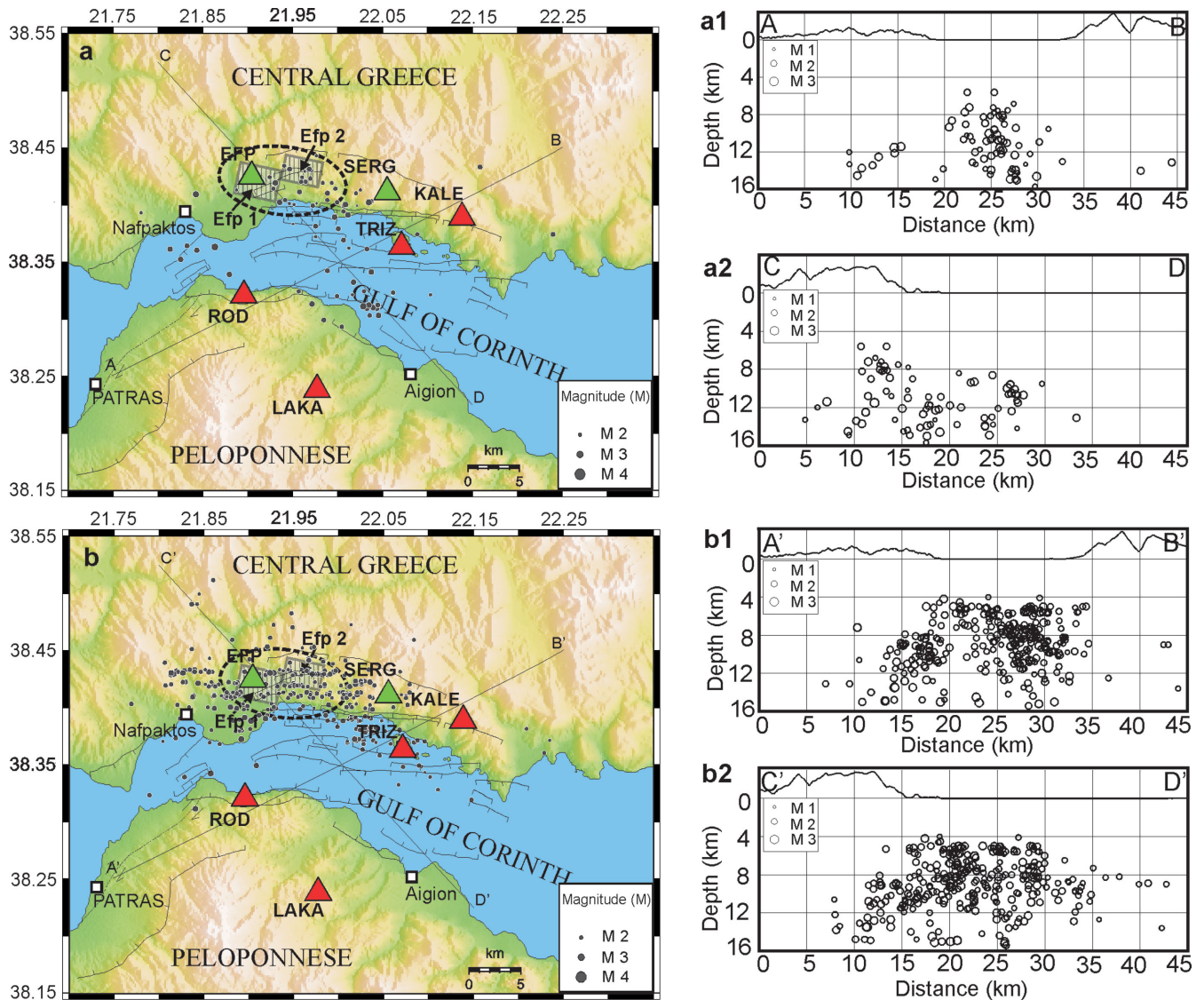
Figure 3. The distribution of the studied seismic events that occurred before (a) and after (b) the Efpalio earthquakes. Vertical cross-sections along the study area depicting the previous seismicity are also presented (a1, a2, b1, b2). The shaded rectangles represent the projections on the surface of the rupture areas of the Efpalio earthquakes (Efp1 and Efp2). The approximate dimensions of the rupture areas were calculated according to Wells & Coppersmith (1994). The dashed ellipses were created for the need of the spatial grouping of the data that are considered to be within and close to the rupture areas. The ellipses were designed approximately according to the slight expansion of the early aftershocks beyond the calculated boundaries of the rupture areas during the first ~30 d after the main shocks following Sokos *et al.* (2012). Seismic stations, major cities and major fault traces are also presented as in Fig. 1.

overview of the results using the complete data set shows that the time-delays estimated for the Period I had a mean value of $2.9 \pm 0.4\,\text{ms}\,\text{km}^{-1}$ while after the Efpalio earthquakes, in Period II, there was an increase to a mean value of $5.5 \pm 0.5\,\text{ms}\,\text{km}^{-1}$. In Period III the mean value of d*t* decreased in $3.6 \pm 0.4\,\text{ms}\,\text{km}^{-1}$. The mean fast polarization direction varied between $68°$ at SERG station, and $125°$ at KALE station, with a mean of $84° \pm 9°$. Fig. 4 shows rose diagrams of the fast shear wave polarization directions as they have been measured during the three subperiods for every single station. The V_P/V_S ratios exhibit an average value of 1.76 ± 0.04 in Period I, while in Periods II and III, the average value significantly increased at 1.88 ± 0.04 and 1.87 ± 0.04, respectively. Table 1 gives a summary showing a list of all the available stations along with the average values of the shear wave splitting parameters. Below, we present in detail the results of this study in accordance with the

aforementioned spatio-temporal grouping of the data that we performed.

3.1 Within and close to the rupture areas

A number of 261 valid splitting measurements derived from seismic events that occurred within and close to the rupture areas of the Efpalio earthquakes. We obtained 42 valid measurements for the Period I, 167 for the Period II and 52 for the Period III. As shown in Fig. 3, EFP station is the only station which is located just above the rupture areas, making in this way the measurements from this station the most representative of the area very close to the rupture zones. Diagrams showing the variation of (a) the measured shear wave time-delays, (b) fast polarization directions and (c) V_P/V_S ratios from this part of the crust are presented in Fig. 5.
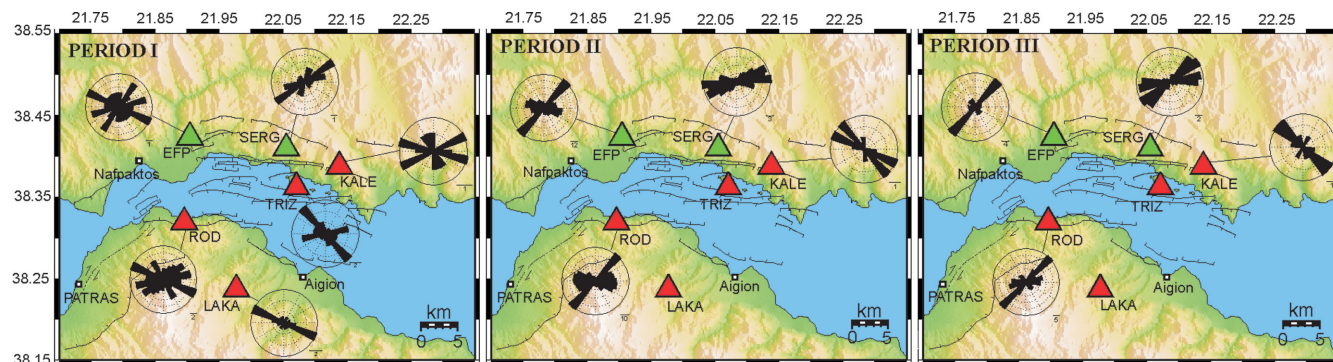
Figure 4. Maps of the western end of the Gulf of Corinth showing rose diagrams of the measured fast shear wave polarization directions. Seismic stations, major cities and major fault traces are also presented as in Fig. 1. [PERIOD I: time period before the 1st Efpalio event (2009 January – Efp1), PERIOD II: time period after the 1st Efpalio event until the end of the aftershock sequence (Efp1 — end of 2010 May) and PERIOD III: time period after the end of the aftershock sequence (2010 June–December)].

Table 1. Summary of the average values of the shear wave splitting parameters measured per seismic station for the whole data set.

Station	Nobs				φ	dt	σ
	Period I	Period II	Period III	Total	(°)	(ms km^{-1})	(ms km^{-1})
EFP	30	136	39	205	75	3.6	4.9
SERG	19	64	46	129	68	6.3	4.2
ROD	16	16	12	44	86	4.2	3.5
KALE	8	8	10	26	125	6.3	4.2
TRIZ	23	–	–	23	122	3.1	2.7
LAKA	12	–	–	12	108	1.2	0.9

Note: Nobs denote the number of observations per station, φ is the mean of the fast polarization directions based on directional statistics, dt is the average time delays normalized according to the hypocentral distance and σ is the standard deviation of these values. Period I: time period before the 1st Efpalio event (January 2009 – Efp1), Period II: time period after the 1st Efpalio event until the end of the aftershock sequence (Efp1 – end of May 2010) and Period III: time period after the end of the aftershock sequence (2010 June–December).

The time-delays estimated for the Period I had a mean value of 2.4 ± 0.5 ms km^{-1} while after the Efpalio earthquakes, in Period II, there was an increase to a mean value of 5.8 ± 0.5 ms km^{-1}. In Period III the mean value of dt slightly decreased to 5.5 ± 0.4 ms km^{-1}. The increase in time-delays is clearly observed soon after the occurrence of the Efpalio earthquakes, exhibiting a decreasing trend a few months later, after the end of the aftershock sequence (see Fig. 5a). For the Period I, fast polarization directions show a mean value of $59° \pm 10°$, while in Periods II and III, the mean values were estimated at $82° \pm 9°$ and $69° \pm 9°$, respectively. The V_P/V_S ratios exhibit an average value of 1.78 ± 0.03 in Period I, while in Periods II and III, the average value significantly increased at 1.89 ± 0.04 and 1.88 ± 0.04, respectively. Corresponding errors for each V_P/V_S ratio have been estimated by using the uncertainties of *P*- and *S*-phase picks. It is noteworthy that average V_P/V_S ratio in Period I is about equal or somewhat lower than the background values estimated by several authors for the same region. For instance, Latorre *et al.* (2004) observed V_P/V_S ratios about 1.78 for the first 15 km of the crust. Rigo *et al.* (1996) and Novotny *et al.* (2012) observed velocity ratios of about 1.83 and 1.80, respectively. We think that the velocity model proposed by Latorre *et al.* (2004) is quite representative for the study area as it was derived during a passive tomography study using seismic events very close to the Efpalio area. The calculated 1.78 ± 0.03 V_P/V_S ratio for Period I is about the same with that estimated from Latorre *et al.* (2004). While the increased observed average V_P/V_S ratios after the Efpalio earthquakes are higher 6.2 per cent for Period II, and 5.6 per cent for Period III than the previously reported value.

3.2 Outside the rupture areas

Focusing on the area outside of the rupture zones of the Efpalio earthquakes, we obtained a total of 178 valid splitting measurements. Specifically, we obtained 43 valid measurements for the Period I, 72 for the Period II and 63 for the Period III. In this case, all seismic stations, except the EFP station, are located outside of the rupture areas (Fig. 3). Diagrams showing the variation of the measured shear wave time-delays (a′), fast polarization directions (b′) and V_P/V_S ratios (c′) from this area are presented in Fig. 5.

Measurements taken from outside the rupture areas show that the time-delays estimated for the Period I had a mean value of 3.4 ± 0.3 ms km^{-1} while after the Efpalio earthquakes, in Period II, there was an increase to a mean value of 5.2 ± 0.4 ms km^{-1}. In Period III the mean value of dt slightly decreased in 4.9 ± 0.4 ms km^{-1}. In this case also, an increase in time-delays is clearly observed soon after the occurrence of the Efpalio earthquakes, exhibiting a decreasing trend a few months later, after the end of the aftershock sequence (Fig. 5a′). For the Period I, fast polarization directions show a mean value of $96° \pm 9°$, while in Periods II and III, the mean values were estimated at $74° \pm 9°$ and $69° \pm 9°$, respectively. The V_P/V_S ratios exhibit an average value of 1.75 ± 0.03 in Period I, while in in both Periods II and III, the average value significantly increased at 1.85 ± 0.04. Similarly to the previous results from the events inside and close to the rupture areas, the average V_P/V_S ratio in Period I is lower than the background values. The calculated V_P/V_S ratio for Period I is lower 1.7 per cent than that estimated from Latorre *et al.* (2004).
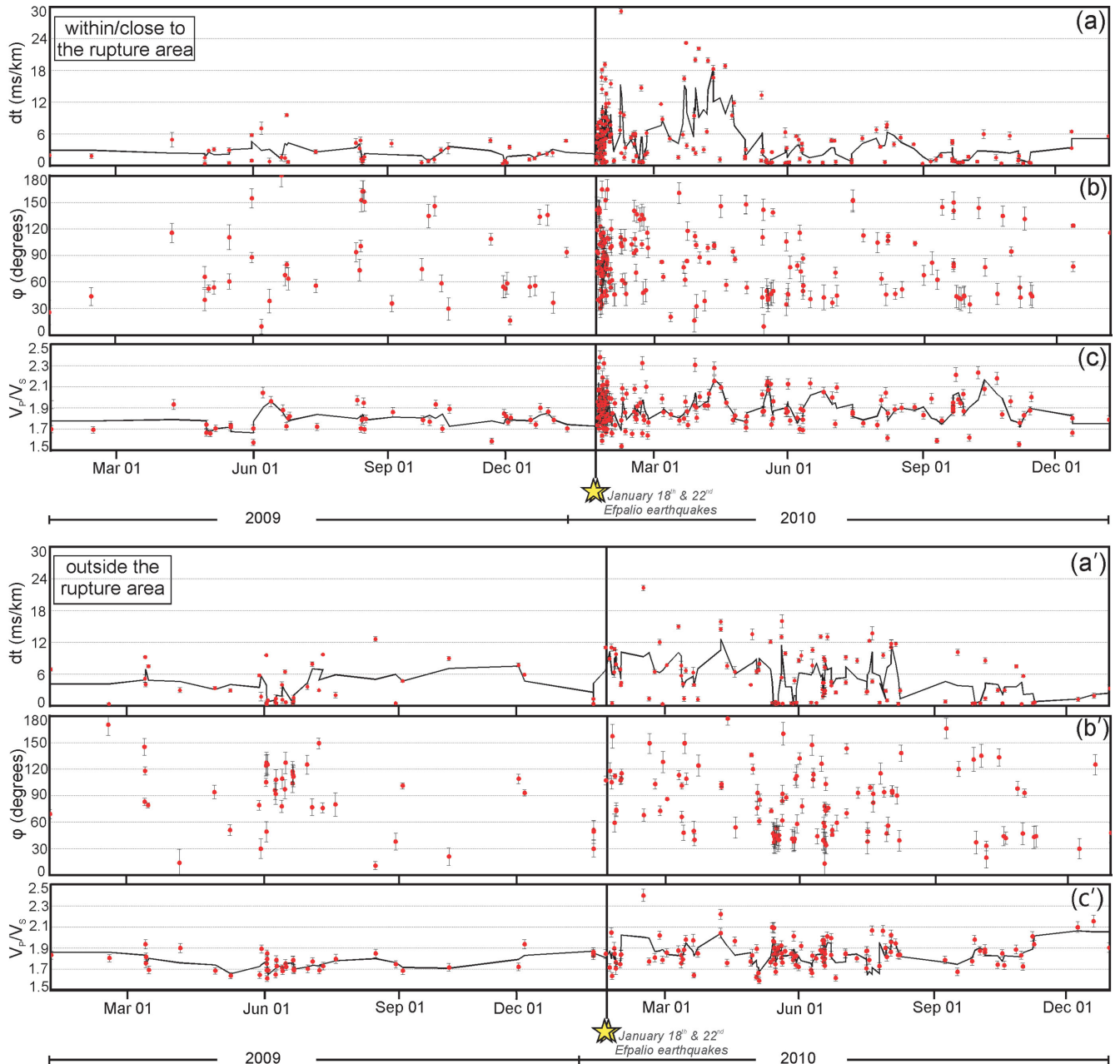
Figure 5. Diagrams showing the variation of the measured shear wave time-delays dt (a and a′), fast polarization directions φ (b and b′) and V_P/V_S ratios (c and c′) with time from events located close/within (top panels) and outside (lower panels) the rupture area. The approximate dimensions of the rupture area are shown in Fig. 2. The time-delays were normalized according to the hypocentral distances. Black vertical bars represent measurement errors. The irregular lines are three-point moving-averages.

While the average V_P/V_S ratios after the Efpalio earthquakes, for both Periods I and II, are higher 3.9 per cent.

3.3 Validation of observations

In order to validate the observed changes of the parameters in time and exclude the possibility that different ray paths bias the measurements values, we followed two procedures. First, we followed a non-parametric hypothesis testing framework. A two-sample Kolmogorov–Smirnov (KS) test was applied to the time-delays and V_P/V_S ratios (Gibbons 1971) and a statistical test appropriate for directional data to the fast polarization directions (Trauth 2010). The statistical tests were applied once between the data sets of Periods

I and II and then between the data sets of Periods II and III, with a level of significance of 5 per cent (for details, see the Appendix). The tests revealed (i) that the difference in time-delays values derived from events inside and close to the rupture zones was significant between the periods before and after the Efpalio earthquakes, (ii) the difference in time-delays values derived from events outside the rupture zones was significant but less stronger than the previous one, (iii) the difference in V_P/V_S values was significant between period I and II, and not for the periods II and III and (iv), that the φ values did not change significantly through the time periods for both the spatial groups of data.

Secondly, we searched our catalogue of the valid measurements for similar earthquakes (hereafter called 'doublets'). We considered
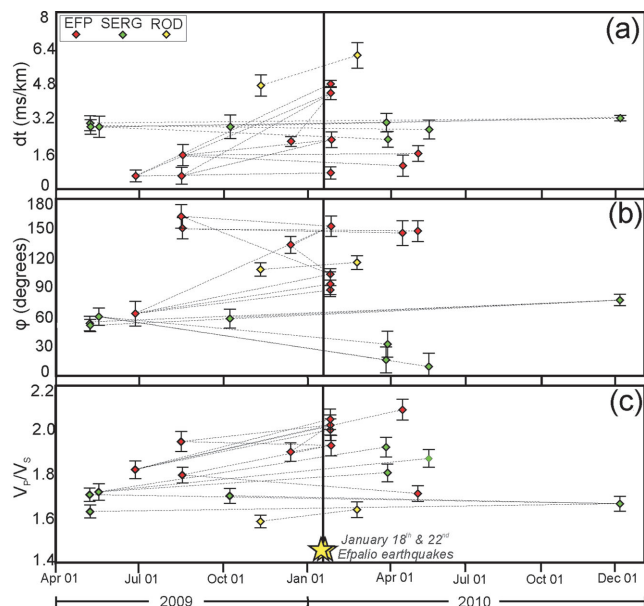
Figure 6. Diagrams showing the variation of (a) the measured shear wave time-delays dt, (b) fast polarization directions φ and (c) V_P/V_S ratios from 2009 January to 2010 December for event doublets. The time-delays were normalized according to the hypocentral distances. Black vertical bars represent measurement errors.

an earthquake doublet as a pair of earthquakes consisting of an earthquake that occurred before the Efpalio events and an earthquake that occurred after that, with a cross-correlation coefficient greater than 0.7, similar magnitude and spaced in distances less than the mean horizontal and vertical location error. A 0.05–5 Hz band-pass filter was used in pre-processing of the seismic waveforms as the waveforms cross-correlation coefficient is more stable at lower frequencies (e.g. Shearer 1997; Shearer *et al.* 2005). Waveforms of seventeen such doublets were found recorded by the EFP, SERG and ROD stations (for details, see supporting information). Fig. 6 shows diagrams with the variation of the measured (a) shear wave time-delays, (b) fast polarization directions and (c) V_P/V_S ratios from 2009 January to 2010 December for event doublets. Considering the time-delay measurements that were obtained from the doublets only, dt had an average value of 1.73 ± 0.4 ms km^{-1} before the Efpalio earthquakes and 2.81 ± 0.4 ms km^{-1} after their occurrence, displaying a relative percentage increment greater than 50 per cent. Fast polarization directions did not exhibit any significant variation before and after the occurrence of the Efpalio earthquakes, as an average direction of 101° ± 11° and 97° ± 9° was obtained, respectively. Finally, concerning the V_P/V_S ratios, an average 1.80 ± 0.037 was measured before and 1.91 ± 0.042 after. Both the application of the statistical testing and the use of doublet earthquakes confirmed the same variation of the initial derived results before and after the Efpalio earthquakes. Table 2 presents a comparison of the average values of all the studied parameters before and after the Efpalio earthquakes as they were derived from the earthquake doublets. According to the previous findings we suggest that our observation shows a robust temporal variation of the time-delays and V_P/V_S during the years 2009–2010.

Diagrams showing the variation of the measured parameters (dt, φ and V_P/V_S ratios) from 2009 January to 2010 December, as well as the results of the statistical testing are presented separately for each station in the supporting information (Figs S1–S3).

Table 2. Comparison of the average values of the studied parameters (φ, dt, V_P/V_S, V_P and Vs) before and after the Efpalio earthquakes, derived from the earthquake doublets.

Parameters	Before Efpalio sequence	After Efpalio sequence	Percentage of relative change
φ (°)	101	97	
dt (ms km^{-1})	1.73	2.81	+53 per cent
V_P/V_S	1.80	1.91	+5 per cent
V_P (km s^{-1})	6.01	6.11	+0.5 per cent
Vs (km s^{-1})	3.34	3.21	−5 per cent

Note: φ is the mean of the fast polarization directions based on directional statistics, dt is the average time delays, V_P and Vs are the *P*- and *S*-velocity, respectively.

4 INTERPRETATION AND DISCUSSION

4.1 Stress field and fast polarization directions

The Gulf of Corinth is considered as one of the most representative and extensively studied areas of active extensional deformation in the world. According to Kokkalas *et al.* (2006), the extension of the gulf is mainly controlled by WNW and ENE-striking normal faults. Stress tensor analysis in the Gulf of Corinth, presented in the previous study, shows a σ_3-axis in a nearly N–S direction (Fig. 1, also see fig. 4 of Kokkalas *et al.* 2006). Small deviation from this general direction is due to the prevalence of one of these two main fault sets. The zones at the junction between the WNW- and ENE-striking faults seem to be notable in terms of the Gulf of Corinth's seismicity. Areas near the bend of the two fault orientations, acted as initiators of moderate to large earthquakes at the past (e.g. the 1993 M_S 5.6 Patras earthquake and the 1981 Alkionides earthquakes). The computed focal mechanisms of the Epf1 and Efp2 events showed *T*-axis azimuths of 187° and 1°, respectively (Sokos *et al.* 2012), observations that are in agreement in general with the trend of the seismo-tectonic, stress and strain regime of the Gulf of Corinth.

The observed ENE–WSW (84° ± 9°) direction of φ is in a good agreement with the regional stress and strain field. According to the mean values of φ in Periods I, II and III derived from events both from inside and outside the rupture areas, and also taking into account their measurement errors, the fast polarization directions did not reveal any significant change. The Efpalio earthquakes seemed to have little or no influence on this parameter. We suggest that the observed ~E–W fast shear wave polarization direction is caused by pre-existing stress-aligned microcracks, oriented parallel or sub-parallel to the horizontal maximum stress axis, which is parallel to the trend of faulting and perpendicular to the N–S extension of the Gulf of Corinth. The orientation of these microcracks most probably did not change after the Efpalio earthquakes. Previous research studies, such as Evangelidis *et al.* (2011), Edrun *et al.* (2011) and Hatzfeld *et al.* (2001), concentrated on deeper parts of the lithosphere investigating the azimuthal anisotropy in the lower crust and mantle across the Hellenic subduction zone and the Aegean region by performing SKS and surface wave anisotropy analyses. It would be interesting to compare our measurements with fast polarization directions deduced for deeper parts of the lithosphere, however, the network coverage that was used from the previous studies was not dense enough in the broader region of our study area. Possible future measurements from a denser network around the study area combined with the measurements of this work could allow us to study, for instance, the degree of the vertical coherence of deformation in the Gulf of Corinth.

4.2 Possible causes of d*t*, V_P/V_S variations

According to Crampin (1999) the principal cause of time-delays variations is fluid migration along pressure gradients between closely spaced microcracks and pores. The CRL's (http://crlab.eu/) main objective is to investigate the mechanics of active faults in the western Gulf of Corinth, with special emphasis on the role of fluids (e.g. Cornet *et al.* 2004; Bernard *et al.* 2006). Within this framework, Bourouis & Cornet (2009) indicated possible overpressure fluid diffusion processes in the western Gulf of Corinth, related to the seismically activated parts of the crust. The previous authors, utilizing also the hydraulic data from a deep well that intersected the Aigion Fault (Cornet *et al.* 2004), suggested that the overpressure conditions within the normal fault system of the area are possibly due to the fact that the faults act as hydraulic barriers in the direction perpendicular to their strike, preventing the fluid flow. In the case of the Aigion Fault, it has been shown that the fault core is made of a 0.5-m-thick impervious clay zone surrounded by permeable cataclastic zones. Existence of fluids in the cataclastic zones of faults in the western Gulf of Corinth has been documented also from geochemical analysis of the faults gouges (Baud *et al.* 2004; Koukouvelas & Papoulis 2009; Pik & Marty 2009). Other studies that have indicated the presence of fluids in the western Gulf of Corinth and their key role in the development of seismicity are among others Latorre *et al.* (2004), Gautier *et al.* (2006) and Pacchiani & Lyon-Caen (2010). Concerning the findings of the previous studies and the observed time-delays variation that we detected, we suggest that the Efpalio earthquakes caused a change in the properties of the crust, as well as in the pre-existing microcrack system geometry. The observed distinctive increase in the time-delays on one hand, and the maintenance of the same mean fast polarization direction before and after the earthquakes on the other hand, suggest that the cause of the observed variations in the splitting parameters was a possible migration of overpressured fluids through the pre-fractured damage zone of the study area. Based on the fact that the increase in the time-delays after the Efpalio earthquakes derived from the data located close to the rupture zones is slightly more intense than the observed increase from the data located outside the rupture areas, we assume that the degree of the changes in the properties of the crust is stronger close to the rupture zones than away from them. A similar example relating to migration of fluids in an overpressured condition within a pre-fracture zone was examined for the case of the 2009 M_W 6.3 L'Aquila earthquake in central Italy by Di Luccio *et al.* (2010). In summary, the previous study has revealed, among others, diffusion processes of overpressured fluids within the pre-fractured crust following the occurrence of the M_W 6.3 L'Aquila earthquake.

An additional interpretation tool concerning the possible involvement of overpressure fluids in the study area is the V_P/V_S ratios measurements. Due to the sensitivity of V_P/V_S ratios in pore fluids, this parameter is an appropriate tool not only for detecting fluid activities, but also for determining the possible fluid phase (gas or liquid phase). V_P/V_S ratios reflect also the properties of the upper crust, varying with mineral, rock compositions and generally with lithology (Fernandez-Viejo *et al.* 2005). These kinds of changes in lithology occur during much larger timescales than the 2-yr of our data set. For this reason, variation in lithology does not seem to be a decisive factor that can influence the observed variations. Seismic tomography studies in different geological systems, like volcanic and geothermal, were successful to delineate zones of high or low V_P/V_S ratios (e.g. Gunasekera *et al.* 2003; Chiarabba & Moretti 2006 and others). These studies have highlighted the dominant role

of fluids in influencing the values of V_P/V_S where liquids result in high V_P/V_S ratios, by lowering the V_S, while gases shift the ratio to lower values as they affect more the V_P in the rock. In order to investigate in more detail the causes of the increase of V_P/V_S after the Efpalio earthquakes, under the assumption of linear ray paths, we calculated apparent V_P and V_S velocities for the same set of events that had an estimated V_P/V_S ratio. We averaged these values for each of the three subperiods and we also compared them with the background values for the top 15 km of the crust derived from the seismic velocity model of Latorre *et al.* (2004). The averaged values of the measured V_P/V_S, V_P and V_S for each period along with the percentage of their relative change from the background values are shown in Fig. 7. The measurements of the apparent V_P and V_S shows that the observed changes in V_P/V_S ratios after the Efpalio earthquakes were due to an increase in V_P and a decrease in V_S. This observation is reflected from data recorded both from inside and outside of the rupture areas. It is important to mention that despite the aforementioned variations in the V_P and V_S, their values were still higher than the background ones proposed by Latorre *et al.* (2004) (see Fig. 7). The previous observed influence of the fluids in the V_P/V_S ratios was also validated by the averaged apparent V_P and V_S values derived from the doublets. In that case, the values of the calculated apparent velocities (see Table 2) show that the occurrence of the Efpalio earthquakes affected more the V_S values than the corresponding V_P since V_S exhibited a 5.5 per cent decrease after the Efpalio earthquakes, while V_P increased by 0.5 per cent. Based on the observed high V_P/V_S ratios after the Efpalio earthquakes and the fact that V_S is decreasing while V_P is increasing, we infer that pore and cracks space in the overpressured cracked rock is most probably filled with liquid.

Latorre *et al.* (2004) performed a three-dimensional delay travel-time tomography by re-analysing a large updated data set, collected in 1991 during a 2-month passive tomographic experiment. The result of this work was the construction of detailed V_P and V_S images of the upper 11 km of the crust in western Gulf of Corinth. The authors pointed out a quite complex structure, identifying two distinct zones exhibiting different characteristics. A shallow structure between 0 and 5 km and a deeper one between 7 and 11 km. The limit between the two zones (5–7 km) was suggested by the recovery of a large-scale vertical velocity anomaly and an increase in the seismicity rate (see figs 13–16 of Latorre *et al.* 2004). At depths larger than 5–7 km, a significant increase in V_P/V_S ratios was found. Vertical V_P/V_S profiles indicated a possible correlation between the observed V_P/V_S anomalies and earthquake clusters located in the study area. According to Latorre *et al.* (2004), fluid saturation in fractured rocks could explain the high V_P/V_S ratio caused by the increase of V_P and decrease of V_S. More specifically, metamorphic processes involving phyllosilicate rocks may be responsible for the release of structural water by dehydration reactions. Because the previous authors and other studies (e.g. Dornsiepen *et al.* 2001; Xypolias & Koukouvelas 2001, among others) have suggested the presence of phyllosilicate-rich rocks within the studied part of the crust, the high V_P/V_S might be caused by the aforementioned metamorphic processes. One could argue that the fluids might have an alternative origin, suggesting for instance that fluids are possibly upper mantle sourced. A database of helium isotope measurements around Greece and surrounding areas compiled by Pik & Marty (2009) does not seem to support such an explanation for our study area. The results of the previous work show a remarkable absence of mantle-He signal in the Corinth rift fluids. Pik & Marty (2009) interpreted the high proportion of crustal helium in the Gulf of Corinth suggesting that the fault system is rooted in the upper crust and is
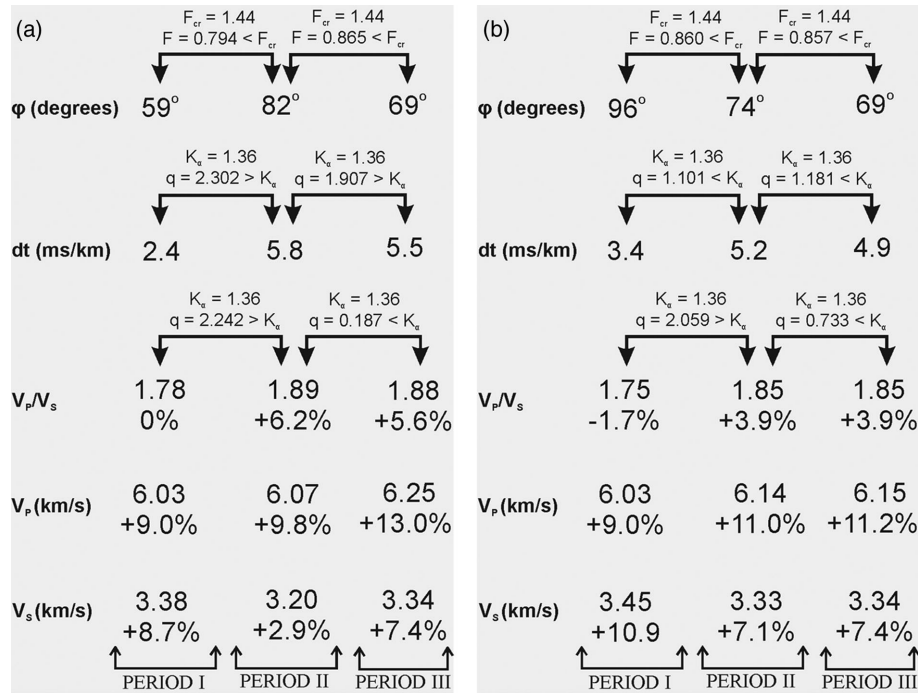
Figure 7. Validation of the variation of the average values of the splitting parameters and V_P/V_S ratios that was observed through the studied time period, after the application of non-parametric hypothesis testing. A two-sample Kolmogorov–Smirnov (KS) test (Gibbons 1971) was applied for the time-delays and V_P/V_S ratios, while a statistical test relative to directional data (Trauth 2010) was applied for the polarization directions (for details about the statistical testing, see the Appendix). The percentage of the relative change between the observed average V_P/V_S ratios, V_P and V_S velocities and the background values derived from the velocity model proposed by Latorre *et al.* (2004) is also shown.

not connected at depth with zones where mantle-He has possibly been trapped.

Pore pressure diffusion in media with hydraulic diffusivity is the main mechanism which controls the triggering and the spatio-temporal evolution of an aftershock seismicity (Shapiro *et al.* 2003). When pore pressure diffusion processes operate, an envelope of cloud of events can be recognized in a plot of the distance of the pressure front from the fluid source versus time. Assuming a homogeneous isotropic medium, the distance of the pressure front from the triggering front (fluid source) can be approximated by the theoretical curve $r = (4\pi Dt)^{1/2}$ where the distance r is a function of the diffusivity D and time t (Shapiro *et al.* 1997; Di Luccio *et al.* 2010). In the case of the Efpalio earthquake sequence, we analysed the aftershocks distribution from the Efp1 up to February 25th. The data used for this analysis consisted of 288 seismic events. The source parameters of the data were provided by Sokos *et al.* (2012). In a distance versus time diagram (r–t) we identify a triggering front with a diffusivity of 4.5 m² s⁻¹ (see Fig. 8). The procedure for fitting the theoretical curve $r = (4\pi Dt)^{1/2}$ to the data was to select the farthest earthquakes that occurred in consecutive, non-overlapping time windows of 5 d, and search using a least squares search the diffusivity (D) value that provided the best fit. The estimated model of the spatio-temporal evolution of the aftershock seismicity (Fig. 8) indicates that the diffusion process started soon after the Efp1 event since it was not observed any time lag between the Efp1 and the triggered earthquakes. The estimated diffusivity value of about 4.5 m² s⁻¹ is within those reported in the literature (e.g. Talwani *et al.* 2007) and, in addition with the observed variation of the V_P/V_S ratios, it strongly supports the involvement of liquid fluids within the fractured medium. For the case of the study of the spatio-temporal evolution of an earthquake swarm occurred in the southern coast of the western Gulf of Corinth (2001 Agios Ioannis
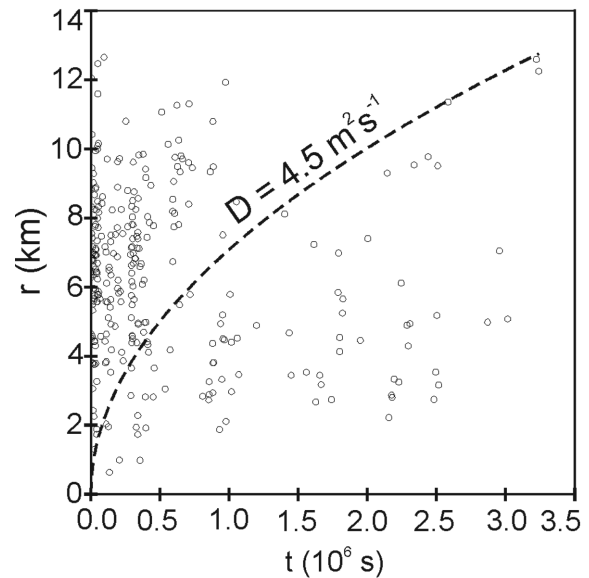

Figure 8. A plot showing the variation of the distances r of the 2010 January 18 to February 25 aftershocks from the focus of the first Efpalio event (2010 January 18) versus their occurrence times t.

earthquake swarm), Pacchiani & Lyon-Caen (2010) estimated a hydraulic diffusivity equal to 0.1 m² s⁻¹. It appears that the fluids in the epicentral area of the Efpalio earthquakes were more diffusible within a possibly more fractured crust. Another comparison can be made with the case of the L'Aquila earthquake, in which Di Luccio *et al.* (2010) estimated a D value of about 4.5 m² s⁻¹ for the foreshocks and a value of 80 m² s⁻¹ for the aftershocks. According to the authors, the value of 80 m² s⁻¹, a threshold value for the

diffusivity of crustal rocks, reflected the involvement of mantle sourced CO_2-rich fluids. The difference between the D values derived from the previous studies and from this work, reflecting different degrees of diffusion processes, is possibly due to the different properties of the fractured crust at the time periods when the studies were conducted and also due to the different magnitudes of the earthquakes of each case. The largest event of the Agios Ioannis earthquake swarm (Pacchiani & Lyon-Caen 2010) had a moment magnitude of 4.3, while the L'Aquila earthquake, as previously mentioned, it was an M_W 6.3 event.

Finally, it is noteworthy to mention the variation of the time-delays in Period III and how it reflects the properties of the crust. After the significant increase that was observed in time-delays after the Efpalio earthquakes, this parameter appears to have a decreasing trend, moving to background values. According to Crampin & Gao (2006), changes of stress affect the geometry of the microcrack system by changing the crack density and aspect-ratios, a process which is directly monitored by variations in average time-delays. It seems possible that the cracks, started to close after the earthquakes due to stress relaxation and the crack density became smaller resulting in smaller values of time-delays.

5 CONCLUSIONS

The results presented in this study can be summarized as follows: (i) shear wave splitting processes were observed in the western end of the Gulf of Corinth during the years of 2009–2010, (ii) fast polarization directions presented a general E–W orientation, which is in agreement with the regional stress and strain field, (iii) fast polarization directions did not change after the Efpalio earthquakes, (iv) a distinct increase in time-delays and V_P/V_S ratios was observed soon after the Efpalio earthquakes, followed by a decrease after the end of the aftershock sequence and (v) after the Efpalio earthquakes, a migration of overpressured liquid fluids through the fractured damage zone is possibly the main cause of the observed increase in time-delays and V_P/V_S ratios. The previous observed variations in the dt and V_P/V_S ratio after the Efpalio earthquakes seemed to be slightly stronger close to the rupture areas than outside of them, which are possibly reflecting different degree of changes in the properties of the crust.

These results provoke the need for further investigations, to study for example in more detail the conditions needed for the presence of overpressured fluids in an area which is characterized by extension and how important could be the role of these fluids in the possibility of generation of slip along low dipping faults. Toward this direction, a time-lapse (4-D) tomography is recommended to be performed as a future work in order to delineate the areas of fluid saturation and their changes over time, since a considerable amount of seismic data recorded during the last ~20 yr in the Corinth Gulf region is available and appropriate for such a study.

REFERENCES

Ando, M., Ishikawa, Y. & Yamazaki, F., 1983. Shear wave polarization anisotropy in the upper mantle beneath Honshu, Japan, *J. geophys. Res.,* **88,** 5850–5864.

Armijo, R., Meyer, B., King, G., Rigo, A. & Papanastassiou, D., 1996. Quaternary evolution of the Corinth Rift and its implications for the Late Cenozoic evolution of the Aegean, *Geophys. J. Int.,* **126**(1), 11–53.

Aster, R., Shearer, P. & Berger, J., 1990. Quantitative measurements of shear-wave polarizations at the Anza seismic network, southern California: implications for shear-wave splitting and earthquake prediction, *J. geophys. Res.,* **95,** 12 449–12 473.

Avallone, A. *et al.*, 2004. Analysis of eleven years of deformation measured by GPS in the Corinth Rift Laboratory area, *Comptes Rend. Geosci.,* **336**(4-5), 301–311.

Baud, P., Diraison, M., Géraud, Y., Reuschlé, T., Schmittbhul, J., Souque, C. & Place, J., 2004. Circulation des fluides dans les systèmes de failles du Rift de Corinthe; Données structurales, pétrophysiques de porosité et de géochimie; rapport GDR "Corinth" (unpublished report, http://crllab.eu/).

Bernard, P. *et al.*, 1997. The Ms = 6.2, June 15, 1995 Aigion earthquake (Greece): evidence for a low-angle normal faulting in the Corinth Rift, *J. Seism.,* **1,** 131–150.

Bernard, P. *et al.*, 2006. Seismicity, deformation and seismic hazard in the western rift of Corinth: new insights from the Corinth Rift Laboratory (CRL), *Tectonophysics,* **426**(1–2), 7–30.

Bourouis, S. & Cornet, F.H., 2009. Microseismic activity and fluid fault interactions: some results from the Corinth Rift Laboratory (CRL), Greece, *Geophys. J. Int.,* **178**(1), 561–580.

Briole, P. *et al.*, 2000. Active deformation of the Corinth rift, Greece: results from repeated Global Positioning System surveys between 1990 and 1995, *J. geophys. Res.,* **105**(B11), 25 605–25 625.

Chiarabba, C. & Moretti, M., 2006. An insight into the unrest phenomena at the Campi Flegrei caldera from V_P and V_P/V_S tomography, *Terra Nova,* **18,** 373–379.

Clarke, P.J. *et al.*, 1998. Crustal strain in central Greece from repeated GPS measurements in the interval 1989–1997, *Geophys. J. Int.,* **135,** 195–214.

Cornet, F.H., Doan, M.L., Moretti, I. & Borm, G., 2004. Drilling through the active Aigion Fault: the AIG10 well observatory, *C. R. Geosci.,* **336,** 395–406.

Crampin, S., 1999. Calculable fluid-rock interactions, *J. Geol. Soc.,* **156,** 501–514.

Crampin, S. & Chastin, S., 2003. A review of shear wave splitting in the crack-critical crust, *Geophys. J. Int.,* **155,** 221–240.

Crampin, S. & Gao, Y., 2005. Comment on "Systematic analysis of shear-wave splitting in the aftershock zone of the 1999 Chi–Chi, Taiwan, earthquake: shallow crustal anisotropy and lack of precursory changes", by Liu, Teng, Ben-Zion, *Bull. seism. Soc. Am.,* **95,** 354–360.

Crampin, S. & Gao, Y., 2006. A review of techniques for measuring shear-wave splitting above small earthquakes, *Phys. Earth. planet. Inter.,* **159,** 1–14.

Crampin, S. & Gao, Y., 2012. Plate-wide deformation before the Sumatra-Andaman Earthquake, *J. Asian Earth Sci.,* **46,** 61–69.

Crampin, S. & Peacock, S., 2005. A review of shear-wave splitting in the compliant crack-critical anisotropic, *Earth Wave Motion,* **41,** 59–77.

Crampin, S., Booth, D.C., Evans, R., Peacock, S. & Fletcher, J.B., 1990. Changes in shear wave splitting at Anza near the time of the North Palm Springs Earthquake, *J. geophys. Res.,* **95,** 11 197–11 212.

Crampin, S., Booth, D.C., Evans, R., Peacock, S. & Fletcher, J.B., 1991. Comment on "Quantitative measurements of shear wave polarizations at the Anza seismic network, Southern California: implications for shear wave splitting and earthquake prediction" by R.C. Aster, P.M. Shearer and J. Berger, *J. geophys. Res.,* **96,** 6403–6414.

Di Luccio, F., Ventura, G., Di Giovambattista, R., Piscini, A. & Cinti, F.R., 2010. Normal faults and thrusts reactivated by deep fluids: the 6 April 2009 M_W 6.3 L'Aquila earthquake, central Italy, *J. geophys. Res.,* **115,** B06315, doi:10.1029/2009JB007190.

Dornsiepen, U.F., Manutsoglu, E. & Mertmann, D., 2001. Permian-Triassic paleogeography of the external Hellenides, *Palaeogeog. Palaeoclimat. Palaeoecol.,* **172,** 327–338.

Doutsos, T. & Kokkalas, S., 2001. Stress and deformation patterns in the Aegean region, *J. Struct. Geol.,* **23,** 455–472.

Doutsos, T. & Poulimenos, G., 1992. Geometry and kinematics of active faults and their seismotectonic significance in the western Corinth-Patras rift (Greece), *J. Struct. Geol.,* **14**(6), 689–699.

Edrun, B., Lebedev, S., Meier, T., Tirel, C. & Friederich, W., 2011. Complex layered deformation within the Aegean crust and mantle revealed by seismic anisotropy, *Nat. Geosci.,* **4,** 203–207.

Evangelidis, C.P., Liang, W.-T., Melis, N.S. & Konstantinou, K.I., 2011. Shear wave anisotropy beneath the Aegean inferred from SKS splitting observations, *J. geophys. Res.,* **116,** B04314, doi:10.1029/2010JB007884.

Fernandez-Viejo, G., Clowes, R.M. & Welford, J.K., 2005. Constraints on the composition of the crust and uppermost mantle in northwestern Canada: V_P/V_S variations along Lithoprobe's SNorCLE, *Can. J. Earth Sci.,* **42,** 1205–1222.

Flotté, N., Sorel, D., Müller, C. & Tensi, J., 2005. Along strike changes in the structural evolution over a brittle detachment fault: example of the Pleistocene Corinth-Patras rift (Greece), *Tectonophysics,* **403**(1–4), 77–94.

Ganas, A., Chousianitis, K., Batsi, E., Kolligri, M., Agalos, A., Chouliaras, G. & Makropoulos, K., 2013. The January 2010 Efpalion earthquakes (Gulf of Corinth, Central Greece): earthquake interactions and blind normal faulting, *J. Seismol.,* **17**(2), 465–484.

Gao, Y. & Crampin, S., 2004. Observations of stress relaxation before earthquakes, *Geophys. J. Int.,* **157,** 578–582.

Gautier, S., Latorre, D., Virieux, J., Deschamps, A., Skarpelos, C., Sotiriou, A., Serpetsidaki, A. & Tselentis, A., 2006. A new passive tomography of the Aigion area (Gulf of Corinth, Greece) from the 2002 dataset, *Pure Appl. Geophys.,* **163**(2), 431–453.

Gibbons, J.D., 1971. *Nonparametric Statistical Inference,* McGraw-Hill.

Gunasekera, R.C., Foulger, G.R. & Julian, B.R., 2003. Reservoir depletion at the Geysers geothermal area, California, shown by four-dimensional tomography, *J. geophys. Res.,* **108,** 2134, doi:10.1029/2001JB000638.

Hatzfeld, D. *et al.*, 1996. The Galaxidi earthquake of 18 November, 1992: a possible asperity within the normal fault system of the Gulf of Corinth (Greece), *Bull. seism. Soc. A.,* **86,** 1987–1991.

Hatzfeld, D., Martinod, J., Bastet, G. & Gautier, P., 1997. An analog experiment for the Aegean to describe the contribution of the gravitational potential energy, *J. geophys. Res.,* **102,** 649–659.

Hatzfeld, D. *et al.*, 2001. Shear wave anisotropy in the upper mantle beneath the Aegean related to internal deformation, *J. geophys. Res.,* **106**(B12), 30 737–30 753.

Jackson, J.A., 1994. Active tectonics of the Aegean region, *Annu. Rev. Earth planet. Sci. Lett.,* **22,** 239–271.

Jackson, J.A., Gagnepain, J., Houseman, G., King, G., Papadimitriou, P., Soufleris, P. & Virieux, J., 1982. Seismicity, normal faulting and the geomorphological development of the Gulf of Corinth (Greece): the Corinth earthquakes of February and March 1981, *Earth planet. Sci. Lett.,* **57,** 377–397.

Karakostas, B. *et al.*, 1994. The aftershock sequence of July 14, 1993 (M_S = 5.4) Patras earthquake, in *Seventh Congress of Geological Society,* Greece, XXX/5, pp. 167–174.

Karakostas, V., Karagianni, E. & Paradisopoulou, P., 2012. Space–time analysis, faulting and triggering of the 2010 earthquake doublet in western Corinth Gulf, *Nat. Hazard,* **63,** 1181–1202.

Kokkalas, S., Xypolias, P., Koukouvelas, I.K. & Doutsos, T., 2006. Post-collisional contractional and extensional deformation in the Aegean region, in *Post-Collisional Tectonics and Magmatism in the Mediterranean region and Asia,* pp. 97–123, eds Dilek, Y. & Pavlides, S., Geological Society of America Special Paper 409.

Koukouvelas, I.K. & Papoulis, D., 2009. Fluid involvement in the He-like normal fault, Gulf of Corinth Greece, *J. Struct. Geol.,* **31,** 237–250.

Kuo, B.Y., Chen, C.C. & Shin, T.C., 1994. Split S waveforms observed in northern Taiwan: implications for crustal anisotropy, *Geophys. Res. Lett.,* **21,** 1491–1494.

Latorre, D., Virieux, J., Monfret, T., Monteiller, V., Vanorio, T., Got, J.L. & Lyon-Caen, H., 2004. A new seismic tomography of Aigion area (Gulf of Corinth, Greece) from the 1991 data set, *Geophys. J. Int.,* **159**(3), 1013–1031.

Le Pichon, X. & Angelier, J., 1979. The Hellenic arc and trench system: a key to the neotectonic evolution of the eastern Mediterranean area, *Tectonophysics,* **60,** 1–42.

Le Pichon, X., Chamot-Rooke, N., Lallemant, S., Noomen, R. & Veis, G., 1995. Geodetic determination of the kinematics of the central Greece with respect to Europe: implication for eastern Mediterranean tectonics, *J. geophys. Res.,* **100,** 12 675–12 690.

Liu, Y., Teng, T.-L. & Ben-Zion, Y., 2004. Systematic analysis of shear-wave splitting in the aftershock zone of the 1999 Chi–Chi, Taiwan, earthquake: shallow crustal anisotropy and lack of precursory changes, *Bull. seism. Soc. Am.,* **94,** 2330–2347.

Liu, Y., Ben-Zion, Y. & Teng, T.-L., 2005. Reply to "Comments on 'Systematic analysis of shear-wave splitting in the aftershock zone of the 1999 Chi–Chi, Taiwan, Earthquake: shallow crustal anisotropy and lack of precursory changes' by Y. Liu, T.-L. Teng, Y. Ben-Zion" by S. Crampin, Y. Gao, *Bull. seism. Soc. Am.,* **95,** 361–366.

McClusky, S. *et al.*, 2000. Global Positioning System constraints on the plate kinematics and dynamics in the eastern Mediterranean and Caucasus, *J. geophys. Res.,* **105,** 5695–5719.

Munson, C.G., Thurber, C.H., Li, Y. & Okubo, P.G., 1995. Crustal shear wave anisotropy in southern Hawaii: spatial and temporal analysis, *J. geophys. Res.,* **100,** 20 367–20 377.

Novotny, O., Sokos, E. & Plicka, V., 2012. Upper crustal structure of the western Corinth Gulf, Greece, inferred from arrival times of the January 2010 earthquake sequence, *Stud. Geophys. Geod.,* **56,** doi:10.1007/s11200-011-0482-7.

Nur, A., 1972. Dilitancy, pore fluids and premonitory variations of ts/tp travel times, *Bull. seism. Soc. Am.,* **62,** 1217–1222.

Pacchiani, F. & Lyon-Caen, H., 2010. Geometry and spatio-temporal evolution of the 2001 Agios Ioanis earthquake swarm (Corinth Rift, Greece), *Geophys. J. Int.,* **180**(1), 59–72.

Papadopoulos, G.A., 2000. A new tsunami catalogue of the Corinth Rift: 373 B.C.–A.D. 2000, in *Historical Earthquakes and Tsunamis in the Corinth Rift,* pp. 121–126, ed. Papadopoulos, G.A., Central Greece, Inst. Geodynamics, Natl. Observatory.

Papanikolaou, D., Chronis, G., Lykousis, V., Sakellariou, D. & Papoulia, I., 1997. Submarine neotectonic structure of W. Korinthiakos Gulf and geodynamic phenomena of the Egion earthquake, in *Proceedings of 5th Hellenic Congress of Oceanography & Fisheries,* Vol. I, Kavala, Greece, pp. 415–418.

Peacock, S., Crampin, S., Booth, D.C. & Fletcher, J.B., 1988. Shear-wave splitting in the Anza seismic gap, southern California: temporal variations as possible precursors, *J. geophys. Res.,* **93,** 3339–3356.

Peng, Z. & Ben-Zion, Y., 2005. Spatiotemporal variations of crustal anisotropy from similar events in aftershocks of the 1999 M 7.4 Izmit and M 7.1 Düzce, Turkey, earthquake sequences, *Geophys. J. Int.,* **160,** 1027–1043.

Pik, R. & Marty, B., 2009. Helium isotopic signature of modern and fossil fluids associated with the Corinth rift fault zone (Greece): implication for fault connectivity in the lower crust, *Chem. Geol.,* **266,** 67–75.

Rigo, A., Lyon-Caen, H., Armijo, R., Deschamps, A., Hatzfeld, D., Makropoulos, K., Papadimitriou, P. & Kassaras, I., 1996. A microseismic study in the western part of the Gulf of Corinth (Greece): implications

for large-scale normal faulting mechanisms, *Geophys. J. Int.,* **126**(3), 663–688.

Seher, T. & Main, I.G., 2004. A statistical evaluation of a "stress-forecast" earthquake, *Geophys. J. Int.,* **157**, 187–193.

Shapiro, S.A., Huenges, E. & Borm, G., 1997. Estimating the crust permeability from fluid-injection-induced seismic emission at the KTB site, *Geophys. J. Int.,* **131**, F15–F18.

Shapiro, S.A., Patzig, R., Rothert, E. & Rindschwentner, J., 2003. Triggering of seismicity by pore-pressure perturbations: Permeability-related signatures of the phenomenon, *Pure appl. Geophys.,* **160**, 1051–1066, doi:10.1007/PL00012560.

Shearer, P.M., 1997. Improving local earthquake locations using the L1 norm and waveform cross correlation: application to the Whittier Narrows, California, aftershock sequence, *J. geophys. Res.,* **102**, 8269–8283.

Shearer, P.M., Hauksson, E. & Lin, G.Q., 2005. Southern California hypocenter relocation with waveform cross-correlation. Part 2: results using source-specific station terms and cluster analysis, *Bull. seism. Soc. Am.,* **95**, 904–915.

Sokos, E. *et al.*, 2012. The January 2010 Efpalio earthquake sequence in the western Corinth Gulf (Greece), *Tectonophysics,* **530–531**, 299–309.

Talwani, P., Chen, L. & Gahalaut, K., 2007. Seismogenic permeability, k_s, *J. geophys. Res.,* **112**, B07309, doi:10.1029/2006JB004665.

Trauth, S.N., 2010. *Matlab® Recipes for Earth Sciences,* 3rd edn, Springer-Verlag.

Tselentis, G., Melis, N. & Sokos, E., 1994. The Patras (July 14, 1993; Ms = 5.4) earthquake sequence, in *Seventh Congress Geological Society,* Greece XXX/5, pp. 159–166.

Tselentis, G., Melis, N., Sokos, E. & Papatsimpa, K., 1996. The Egion June 15, 1995 (6.2 Ml) earthquake, Western Greece, *Pure appl. Geophys.,* **147**, 83–98.

Valkaniotis, S., 2009. Correlation between Neotectonic structures and Seismicity in the broader area of Gulf of Corinth (Central Greece), *PhD thesis,* Aristotle University of Thessaloniki, Thessaloniki.

Wells, D.L. & Coppersmith, K.J., 1994. New empirical relationships among magnitude, rupture length, rupture width, rupture area and surface displacement, *Bull. seism. Soc. Am.,* **84**(4), 974–1002.

Wessel, P. & Smith, W.H.F., 1998. New improved version of the Generic Mapping Tools Released, *EOS, Trans. Am. geophys. Un.,* **79**, 579.

Xypolias, P. & Koukouvelas, I., 2001. Kinematic vorticity and strain rate patterns associated with ductile extrusion in the Chelmos Shear Zone (External Hellenides, Greece), *Tectonophysics,* **338**, 59–77.

APPENDIX: STATISTICAL TESTING

A1 Two-sample Kolmogorov–Smirnov test

In the geosciences, there are a lot of occasions where we want to test the hypothesis that two data sets derive from the same statistical distribution. However, the kind and sizes of the samples do not allow any assumption about their distribution (e.g. Gaussian distributed). In these cases, we need a non-parametric two-sample statistical test for checking this hypothesis. Such a test is the two-sample Kolmogorov–Smirnov (KS) test (Gibbons 1971). The two-sample KS test is one of the most used and general non-parametric method for comparing two populations, as it is sensitive to differences in both the location and shape of the empirical cumulative distribution functions of the two samples. Specifically, let us assume X_1, X_2, two data sets, of length n and m, respectively, and let $F_{1,n}(x)$, $F_{2,m}(x)$ be their empirical distributions. We need to test under what circumstances the hypothesis $F_{1,n}(x) = F_{2,m}(x)$ (the null hypothesis) is valid. In this case, the KS statistic is:

$$D_{n,m} = \sup_x \left| F_{1,n}(x) - F_{2,m}(x) \right| \tag{A1}$$

and the null hypothesis is rejected, with a level of significance α if:

$$q = \sqrt{\frac{nm}{n+m}} D_{n,m} > K_a, \tag{A2}$$

where K_a is a constant threshold value that is derived from the Kolmogorov distribution. We applied this hypothesis-testing procedure in V_P/V_S ratios and time delays data, with a significance level $a = 5$ per cent.

A2 *F* statistic test for directional data

Let us consider: θ_1, θ_2, ..., θ_n and φ_1, φ_2, ..., φ_m as the two sets of azimuth measurements. We wish to statistically test the hypothesis that they belong to the same distribution. Before using the appropriate statistic, a specific analysis relative to the directional data has to be followed (Trauth 2010). The characteristics of the directional data are described by measures of central tendency and dispersion, which are similar to the statistical characterization of univariate data sets. Initially, we need to calculate the resultant or mean direction for the sets of angular data according to the relationships:

$$x_{1r} = \sum \sin \theta_\iota \tag{A3}$$

$$y_{1r} = \sum \cos \theta_\iota \tag{A4}$$

and

$$x_{2r} = \sum \sin \varphi_\iota \tag{A5}$$

$$y_{2r} = \sum \cos \varphi_\iota. \tag{A6}$$

The resultant directions of the data are given by:

$$\bar{\theta} = \tan^{-1}\left(\frac{x_{1r}}{y_{1r}}\right) \tag{A7}$$

and

$$\bar{\varphi} = \tan^{-1}\left(\frac{x_{2r}}{y_{2r}}\right) \tag{A8}$$

and the mean resultant lengths are:

$$R_1 = \frac{1}{n}\sqrt{(x_{1r}^2 + y_{1r}^2)} \tag{A9}$$

and

$$R_2 = \frac{1}{m}\sqrt{(x_{2r}^2 + y_{2r}^2)}, \tag{A10}$$

respectively.

The test statistic that we used for testing the similarity between the two mean directions is the *F*-statistic, and it is given by the relationship:

$$F = \left(1 + \frac{3}{8k}\right)\frac{(N-2)(R_1 + R_2 - R_{\text{all}})}{N - R_1 - R_2}, \tag{A11}$$

where k is the concentration parameter, which can be obtained from tables using R_{all}, R_1 and R_2 are the mean directions (resultants) of the two data sets, respectively, and R_{all} is the resultant of the combined data sets. The calculated *F*-statistic is compared with the critical values from the standard *F* tables, and the two mean directions are not significantly different if the measured *F*

is lower than the critical F_{cr}. As previously, we applied the aforementioned statistical test to our data with a level of significance 5 per cent.

SUPPORTING INFORMATION

Additional Supporting Information may be found in the online version of this article:

Figure S1. Diagrams showing the variation of the measured shear-wave time-delays dt (a), fast polarization directions φ (b) and V_P/V_S ratios (c) from all the available data recorded between January 2009 and December 2010 per station. The time-delays were normalized according to the hypocentral distances. Black vertical bars represent measurement errors. The names of the stations are shown at the top left corner of each panel.

Figure S2. Diagrams showing the variation of the measured shear-wave non-normalized time-delays dt per station. Black vertical bars represent measurement errors. The names of the stations are shown at the top left corner of each panel.

Figure S3. Application of non-parametric hypothesis testing on the average values of the splitting parameters and V_P/V_S ratios. A two-sample Kolmogorov–Smirnov (KS) test (Gibbons 1971) was applied for the time-delays and V_P/V_S ratios, while a statistical test relative to directional data (Trauth 2010) was applied for the polarization directions. The percentage of the relative change between the observed average V_P/V_S ratios, V_P and V_S velocities and the background values derived from the velocity model Latorre *et al.* (2004) is shown also.

Figure S4. Diagrams showing the variation of the measured shear-wave non-normalized time delays dt with time. Black vertical bars represent measurement errors.

Figure S5. Equal area projections of the fast polarization directions. (a) whole time period (January 2009–December 2010), (a1) time period before the 1st Efpalio event (January 2009 – Efp1 (January 18, 2010)), (a2) time period after the 1st Efpalio event until the end of the aftershock sequence (Efp1 – end of May 2010) and (a3) time period after the end of the aftershock sequence (June 2010–December 2010). The radius of the plots is scaled to an incidence angle of 45° (effective shear-wave window (Booth & Crampin 1987)).

Figure S6. (a) & (b) Waveforms of 'earthquake doublets' or 'similar earthquakes' recorded by the EFP, SERG and ROD stations. We considered the similar earthquakes/earthquake doublets as a pair of earthquakes consisting of an earthquake that occurred before the Efpalio events and an earthquake that occurred after that, with a cross-correlation coefficient greater than 0.7, similar magnitude and spaced in distances less than the mean horizontal and vertical location error. A 0.05–5 Hz band-pass filter was used in pre-processing of the seismic waveforms as the waveforms cross-correlation coefficient is more stable at lower frequencies (e.g. Shearer 1997; Shearer *et al.* 2005).

Table S1. Data availability for the studied time period. Months with at least some data are plotted in grey.

Table S2. Pairs of earthquake doublets with the corresponding splitting parameters (φ and dt) as well as the corresponding values of V_P/V_S ratio, V_P and V_S. (http://gji.oxfordjournals.org/lookup/suppl/doi:10.1093/gji/ggu467/-/DC1).

Please note: Oxford University Press is not responsible for the content or functionality of any supporting materials supplied by the authors. Any queries (other than missing material) should be directed to the corresponding author for the article.